Naval Surface Warfare Center
Carderock Division
West Bethesda, MD 20817-5700

NSWCCD-TR-61–98/33 November 1998

Survivability, Structures, and Materials Directorate

Technical Report

Factors Affecting the Strength and Toughness of Low Carbon Alloy Steel Weld Metal

by

J. M. Blackburn

NSWCCD-TR-61–98/33 Factors Affecting the Strength and Toughness of Low Carbon Alloy Steel Weld Metal

REPORT DOCUMENTATION PAGE

Form Approved
OMB No. 0704-0188

1. AGENCY USE ONLY *(Leave blank)*	2. REPORT DATE	3. REPORT TYPE AND DATES COVERED
	18 November 1998	Research and Development 971001-980931

4. TITLE AND SUBTITLE
Factors Affecting the Strength and Toughness of Low Carbon Alloy Steel Weld Metal

5. FUNDING NUMBERS
1-6150-853

6. AUTHOR(S)
J.M. Blackburn

7. PERFORMING ORGANIZATION NAME(S) AND ADDRESS(ES)
NAVAL SURFACE WARFARE CENTER
CARDEROCK DIVISION (CODE 615)
9500 MACARTHUR BOULEVARD
WEST BETHESDA, MD 20817-5700

8. PERFORMING ORGANIZATION REPORT NUMBER
NSWCCD-TR–61-98/33

9. SPONSORING/MONITORING AGENCY NAME(S) AND ADDRESS(ES)
OFFICE OF NAVAL RESEARCH (CODE 332)
BALLSTON CENTRE TOWER ONE
800 NORTH QUINCY STREET
ARLINGTON VA 22217-5000

10. SPONSORING/MONITORING AGENCY REPORT NUMBER

11. SUPPLEMENTARY NOTES

12a. DISTRIBUTION/AVAILABILITY STATEMENT
Approved for public release; distribution is unlimited.

12b. DISTRIBUTION CODE

13. ABSTRACT ***(Maximum 200 words)***

This report details a metallurgical analysis which identifies the factors affecting the strength and toughness behavior of newly developed low carbon welding consumables. It was found that the 50% transformation temperature (T_{50}) was a good indicator of the microstructure type and was successfully correlated to weld deposit strength. Other factors responsible for strength development were prior austenite grain width (γ_{gw}), cooling rate, multipass reheating, carbon content and oxygen. The factors responsible for toughness development (@-51°C) were the yield to ultimate strength ratio, cooling rate, oxygen and carbon contents. The austenite grain width and 50% transformation temperature were modeled from welding parameters and weld deposit composition, permitting successful prediction of weld metal strength and toughness. The optimum weld deposit compositions as determined by the model was 0.04%C, 0.60% Mo, 2.4%Ni, and 0.4% Si if the oxygen content was 200ppm, and 0.04%C, 0.60% Mo, 2.6%Ni, and 0.4% Si if the oxygen content was 250ppm.

14. SUBJECT TERMS	15. NUMBER OF PAGES
Low Carbon Alloy Steel Weld Metal	0
	16. PRICE CODE

17. SECURITY CLASSIFICATION OF REPORT	18. SECURITY CLASSIFICATION OF THIS PAGE	19. SECURITY CLASSIFICATION OF ABSTRACT	20. LIMITATION OF ABSTRACT
UNCLASSIFIED	UNCLASSIFIED	UNCLASSIFIED	SAR

NSN 7540-01-280-5500

Standard Form 298 (Rev. 2-89)
Prescribed by ANSI Std. Z39-18
298-102

TABLE OF CONTENTS

List of Tables

List of Figures

Abstract

This report details a metallurgical analysis which identifies the factors affecting the strength and toughness behavior of newly developed low carbon welding consumables. It was found that the 50% transformation temperature (T_{50}) was a good indicator of the microstructure type and was successfully correlated to weld deposit strength. Other factors responsible for strength development were prior austenite grain width (γ_{gw}), cooling rate, multipass reheating, carbon content and oxygen. The factors responsible for toughness development (@-51°C) were the yield to ultimate strength ratio, cooling rate, oxygen and carbon contents. The austenite grain width and 50% transformation temperature were modelled from welding parameters and weld deposit composition, permitting successful prediction of weld metal strength and toughness. The optimum weld deposit compositions as determined by the model was 0.04%C, 0.60% Mo, 2.4%Ni, and 0.4% Si if the oxygen content was 200ppm, and 0.04%C, 0.60% Mo, 2.6%Ni, and 0.4% Si if the oxygen content was 250ppm.

Acknowledgements

This work was sponsored by ONR, Dr. George Yoder (ONR Code 332). This work was part of the ONR Seaborne Structural Materials Project.

Introduction

Solid wires for GMAW are currently being developed for high strength steels for use in Navy ship applications (550-690 MPa). A full description of the Navy consumable development program can be found elsewhere.[1] Such strength levels are achievable but are quite dependent on weld metal cooling rate and can be associated with poor toughness and hydrogen cracking resistance. The goal for the new consumables under development was to achieve the same strength and toughness levels while reducing the cooling rate sensitivity and eliminating the need for preheating.

During the course of the solid wire development program, the strength/toughness relationship shown in Figure 1 emerged. This relationship developed as a function of chemistry and weld metal cooling rate. In general, as the chemistry became richer, or the cooling rate became faster, the strength increased. Figure 1 shows that low strength is accompanied by low toughness. It also shows that increasing strength increases toughness up through a yield strength of about 600 MPa. Further increases in strength resulted in reduced toughness. The low strength, low toughness regime generally occurred at cooling rates of less than 5°C/s. The peak in the strength/toughness relationship generally occurred near 20°C/s. Increases in cooling rate beyond 20°C/s lead to increased strength and a decrease in toughness. Although it was suspected that this behavior was a result of changing microstructure, it was not fully understood, and thus lead to a metallurgical analysis and model development which will be described in this investigation.

Objective

The objective of this investigation was to determine the factors governing the development of strength and toughness and to quantify these factors with the use of regression analysis tools.

Approach

It has been demonstrated by Pickering[2] that specific microstructural features can be responsible for strength and toughness development in steel alloy systems. They include ferrite and austenite grain width, bainite or martensite packet size, particle size and particle dispersion. It is also known that impurities such as S, P, O and Al can also affect strength and toughness. Although Pickering's work was on plate materials, it was expected that microstructure and impurities similarly affect strength and toughness in weld metal. However, the development of microstructure in weld metal is somewhat different. Weld metal experiences a much broader range of cooling conditions, contains a fine dispersion of oxide inclusions, and can experience localized reheating and recrystallization due to the deposition of multiple weld passes.

Since microstructural features are tedious to measure and difficult to correlate with mechanical properties another approach to describing microstructure was adopted. A more readily measured characteristic is the 50% transformation temperature, T_{50}. Pickering showed that strength was highly dependent on T_{50}. As the transformation temperature was lowered, the strength was increased in a linear fashion for a given type of microstructure. This trend was also expected for these weld metals. Therefore, T_{50} was determined for the alloys under study and related to strength. The correlation which was achieved was significant but was not considered to be accurate enough for alloy design. It was thought that austenite grain width may be responsible for a significant portion of the error. Austenite grain widths (γ_{gw}) were measured and correlated with strength also. The results indicated that γ_{gw} was also a contributing factor. At this point, T_{50} and γ_{gw} were two factors to be considered throughout the development of the strength and toughness models. Other factors which were considered were calculated cooling rate, plate thickness, intentional alloy composition (C, Mn, Si, Mo, Ni, Cr), impurity composition (O, N,P, S, Al, Ti, Al) and various ratios and multiplications such as Si/O, Ti/O, Al/O/ Mn/O, Al/N, Ti/N, Mn/Si, Mn/Mo, C*Mn, C*Si, Mn*Mo, Mn*Ni, etc.

Calculated cooling rate is a convenient term because it incorporates the welding heat input and plate thickness, and thus a single term represents a number of variables (amps, volts, travel speed, plate thickness). The method used in this work for calculating weld metal cooling rates is well documented in the literature by the works of Rosenthal[3], Dorschu[4], and Jhaveri[5].

Since the strength models required T_{50} and γ_{gw}, it was necessary to develop models for these factors also. The models for T_{50} and γ_{gw} required that they relate to composition and welding parameters to allow prediction of properties from composition and welding parameters.

Once the strength models were developed, a similar approach to developing the toughness model was undertaken. The same factors used to investigate correlations with strength were used in search of correlations with toughness. However, in the case of toughness, σ_y and σ_{UTS} were also considered.

The data which will be presented here was not a statistically designed set of experiments. However, statistics were used to support the choice of variables. Terms were rejected on the basis of the p-value (level of significance) and error distribution and not on the standard error. Models were considered acceptable when the regression terms displayed p-values of ≤ 0.10 and when residual error distribution was normal.

Procedures

Welding Details and Mechanical Properties.

Fifty-two welds were fabricated with 7 different solid wires. All welds were prepared with the GMAW process (spray or pulsed) using 95%Ar-5% CO_2 shielding gas. Welds were prepared in HSLA-100, HSLA-80, and HY-80 plate with thicknesses ranging from 1cm to 5cm and various heat inputs/cooling rate conditions. The combination of 7 welding wires, various heat inputs and 3 baseplate materials provided for a wide range of weld metal compositions, mechanical properties, γ_{gw}, and T_{50}. The ranges of composition and properties are given in Table 1. Appendices 1 and 2 contain a complete data set for all welds produced and tested in this investigation.

Tensile testing was performed on all weldments. Two all weld metal tensile specimens were removed from each weldment. Specimens of 6 mm or 13 mm diameter were removed in the longitudinal orientation and the 0.2% offset yield strength and ultimate tensile strength calculated from the engineering stress-strain diagram. In all cases, the test region length to diameter ratio was kept at a value of 4:1.

Standard Charpy Vee-Notch specimens were also removed from all weldments. Three specimens each were tested at -18°C and -51°C. The model development described herein addresses specimens tested at -51°C only.

Optical Metallography and Hardness

Optical metallography was performed on selected weldments. Specimens were etched in a 50% mix of 4% picral and 2% nital solution. Specimens were examined to determine the as-deposited microstructure and the reheated microstructure.

Determination of the 50% Transformation Temperature, T_{50}

Specimens approximately 12 mm long were sectioned from remaining sections of the tensile specimens. These specimens were placed in the Gleeble 1500 weld thermal cycle simulator. The Rykaline 3-dimensional thermal model was used to produce the desired thermal profile and cooling rate. A peak temperature of 1200°C and no hold time was used for each thermal cycle. The specimens were held in slight compression between the copper jaws of the Gleeble, as shown in Figure 2. The calculated weld cooling rates were rounded to the nearest of the following cooling rates for simulation on the Gleeble: 1,10,20,30,40,60 and 70°C/s. Each specimen was then subjected to a thermal cycle similar to its original weld thermal profile. During the thermal cycling, a dilatometer was placed on the diameter of the specimen to record expansion and contraction.

Figure 3 displays a representative plot of temperature versus dilation during the cooling cycle, and associated analysis of partial transformations. Figure 3 is a portion of the whole dilatometer plot during the cooling cycle. The linear portions represent the response due to thermal contraction and are proportional to the coefficient of thermal expansion. These lines were determined using a least squares fit. The areas that deviate from linearity are due to the volumetric expansion associated with the phase transformations. The first point where the curve deviates from linearity upon cooling is the start of transformation, and the return to linearity is the finish of transformation. Once the lines representing the coefficient of thermal expansion were determined for austenite and the final austenite decomposition product, the lever rule was utilized at each point to determine the percent transformation. At each point, for example, the percent transformation was determined by $(a \times 100)/(a+b)$. The 50% transformation would then be defined when the distance, a,

is equal to distance *b*. Using this methodology the transformation temperatures were determined.

Table 1. Ranges of composition and properties.

	Range	
	Min.	Max.
Plate thickness (cm)	1	5
dT/dt (°C/s)	1	71
σ_y (MPa)	485	873
σ_{uts} (MPa)	622	919
El (%)	11	27
RA (%)	10	82
CVN(-18°C), j	37	351
CVN(-51°C), j	12	301
C (wt.%)	0.016	0.049
Mn (wt.%)	0.780	1.710
Si (wt.%)	0.140	0.350
Cr (wt.%)	0.009	0.230
Ni (wt.%)	2.060	4.670
Mo (wt.%)	0.420	1.330
Cu (wt.%)	0.001	0.300
S (wt.%)	0.001	0.005
P (wt.%)	0.001	0.190
Al (wt.%)	0.001	0.013
Ti (wt.%)	0.002	0.012
O (wt.%)	0.014	0.047
N(wt.%)	0.0004	0.00950
T_{50} (°C)	387	590
γ_{gw}, microns	84	416

Prior Austenite Grain Width (γ_{gw}) Determination

The austenite grain width of as-deposited weld metal was determined. A digital image analysis system was utilized to perform a linear intercept method on selected specimens. Specimens were etched in either a 50% mix of 4% picral and 2% nital solution or saturated picric solution. A minimum of 50 grains, at magnifications of 50 to 200 times, were measured and subsequently averaged.

Results

Optical Microscopy and Hardness

In general, the microstructures within the multi-pass welds consisted of grain boundary ferrite (in as-deposited structures), polygonal ferrite, acicular ferrite, lath ferrite, a very fine martensite-like structure and mixtures containing some or all of these. More specifically, the as-

deposited microstructure at slow cooling rates was primarily large grained polygonal ferrite within a large austenite grain width (See Figure 4). The as-deposited microstructures at intermediate cooling rates contained mixtures of acicular ferrite, polygonal ferrite and lath ferrite (See Figure 5). The microstructure of the as-deposited weld metal at fast cooling rates was a very fine acicular structure resembling martensite with some lath ferrite, and some polygonal and acicular ferrite (See Figure 6). In the reheated regions of the weld metal the microstructure evolved towards a refined polygonal ferrite structure as shown in Figure 7.

This progression from large grained polygonal ferrite to a very fine martensitic structure, as a function of cooling rate, corresponded with a decrease in the 50% transformation temperature. The 50% transformation temperature for the materials illustrated in Figs. 4, 5 and 6 were 590, 510 and 420°C, respectively. These transformation temperatures corresponded with diamond pyramid hardnesses of 208, 257 and 316, respectively.

50% Transformation Temperature, T_{50}

The T_{50} data is plotted against the strength in Figure 8. The data in Figure 8 shows a linear relationship between the T_{50} and the strength values. This is consistent with the work of Pickering on bainitic base plate materials. The data in Figure 8 is identified by the type of optical microstructure observed. A "ferritic" microstructure means that different forms of non-lath and lath ferrite only were observed. The term "martensitic" indicates that the structure contained some or all of the very fine, martensite-like structure. The description "ND" denotes that the optical microstructure was "not determined".

The ferritic structures obtained a maximum σ_y of approximately 630 MPa and a maximum σ_{uts} of approximately 698 MPa. Higher strengths required mixtures of ferrite and martensite structures. When martensite was present, σ_y as high as 896 MPa and σ_{uts} to 1100 MPa were achieved.

A T_{50} of 510°C divided the formation of ferritic structures only and formation of a fine martensitic structure. Above a T_{50} of 510°C ferritic structures only were produced. Below a T_{50} of 510°C mixtures of the martensitic and ferritic structures emerged. It should be noted that some purely ferritic products also displayed a T_{50} at 510°C or lower but did not achieve the same strength levels as the weld metals containing martensite. This could be due to other factors, such as grain size or tempering.

Although a linear trend-line is used to represent the σ_{uts} data, the data with T_{50} greater than 510°C may exhibit a different relationship between T_{50} and σ_{uts}. The "ferritic" data in the σ_{uts} plot of Figure 8 appears to incorporate a different slope than the trend line shown. This indicates that other factors are involved in the correlation. A similar relationship was seen by Irvine and Pickering.[6] Their data showed that different slopes existed for different microstructures, which also appears to be the case for this data. This change in slope was probably due to factors in addition to T_{50}. Therefore, other factors were considered in the regression analaysis, as will be discussed in the "Strength Model" section.

50% Transformation Temperature (T_{50}) Model

Models for determining T_{50} of steel baseplate has been previously developed[7,8] and applied to the data in this work. Upon comparing the calculated values with the measured values, it was found that agreement was only fair to non-existent. The Steven model[7] over-predicted the lower values of T_{50} and under-predicted the higher transformation temperatures. The Andrews model[8] under-predicted all of the data except for the very low temperature data. The performance of these existing models is reasonable because they were developed specifically for bainitic (Steven) and martensitic

(Andrews) microstructures. In the case of this work a wide range of microstructures were encountered. Therefore, a new model was developed to represent the entire microstructural range, as presented in Eqn. 1, which also incorporates cooling rate and oxygen effects.

$$T_{50} = 780\text{-}13\ln(dT/dt)\text{-}1266C\text{-}56Mo\text{-}45Ni\text{-}3.6(Si/O) \qquad \text{Eqn. 1}$$

The fit of the model in Eqn. 1 is shown in Figure 9. The model predicted the T_{50} very well over a large range of temperatures. The T_{50} model indicates that alloying additions and increases in cooling rate depress the transformation temperature. On the other hand, the term (Si/O) indicates that increasing oxygen tends to raise the transformation temperature. This is reasonable since increasing oxygen content promotes the formation of inclusions and hence the nucleation of higher temperature ferritic transformation products. It also indicates that increasing Si depresses the transformation temperature. The model of Eqn. 1 does not include terms for Mn and Cr. The statistics for these two terms were not significant. Although other alloying elements did not prove to be significant factors in the regression analysis, it is believed that elements such as Mn, Ti, and Al served to reduce the oxygen content, therefore decreasing T_{50}.

Prior Austenite Grain Width, γ_{gw}

The effects of γ_{gw} and T_{50} on σ_y are plotted in Figure 10. It is clear that both γ_{gw} and T_{50} had an effect on σ_y. The data indicate that the peak transformation temperature, approximately 580°C, corresponded to an γ_{gw} near 200 microns. The wide range of transformation temperatures for a given γ_{gw} was due to variations in cooling rates. Faster cooling rates for a given γ_{gw} resulted in lower transformation temperatures. It is interesting to note that similar strength levels were obtained with various combinations of grain width and transformation temperatures. This indicates that the transformation strengthening is offset by an increase in austenite grain width. This trend was similar for σ_{uts}.

The trends that existed between alloying and γ_{gw} are presented in Figure 11 through Figure 14. However, it should be noted that this experiment was not a statistical design, and that the trends which are displayed in these figures are not the result of a controlled experiment in which individual alloying elements were isolated. These trends merely served as a starting point in assessing the significance of alloying on γ_{gw}. Regression statistics were used in the model development aspects of this work to further justify the significance of each alloying element.

The effect of carbon and chromium on γ_{gw} are shown in Figure 11. Increasing carbon from 0.02 wt.% to 0.04 wt.%, appeared to reduced the γ_{gw} from 425 microns to less than 100 microns. Chromium appeared to produce a two-fold effect on γ_{gw}. At levels of less than about 0.06 wt.%, increasing chromium reduced grain width. At chromium contents above 0.06 wt.%, increasing chromium appeared to increase grain width.

The effect of manganese and nickel on γ_{gw} are shown in Figure 12. Increasing manganese appeared to decrease γ_{gw}, while the trend with nickel was oscillating. At nickel levels below 3 wt.%, increasing nickel decreased γ_{gw}. Increasing nickel at levels above 3 wt.% increased γ_{gw}.

No obvious correlation existed between oxygen and γ_{gw} when plotting all of the data. A trend did exist when T_{50} was >510°C. This trend is shown in Figure 13. Within this regime, oxygen increased γ_{gw}. For transformation temperatures less than 510°C, the best correlation to γ_{gw} occurred with Ni contents, as shown in Figure 14. The separate correlations of γ_{gw} with oxygen and nickel may explain the oscillitory behavior for Ni in Figure 12. At low levels of Ni the microstructures were non-martensitic. In this case oxygen was controlling γ_{gw}. At higher levels of Ni the microstructure was martensitic. In this case the Ni and Mo were controlling γ_{gw}. This combination of

factors controlling γ_{gw} therefore resulted in a potential misleading trend with Ni.

Prior Austenite Grain Width (γ_{gw}) Model

Two models were necessary to describe γ_{gw}. The regression statistics indicated that when T_{50} was greater than 510°C, oxygen was the sole factor controlling γ_{gw}. When T_{50} was less than or equal to 510°C Ni and Mo were the two factors which correlated with γ_{gw}. The resulting regression equations are presented in Eqns. 2 and 3. Regression analyses suggested that Cr, Mn and C were not significant factors. Figure 15 shows how well the model predicts the actual measured values of the austenite grain width. However, it is believed that elements such as Mn, Ti, and Al served to reduce the oxygen content, therefore decreasing γ_{gw}.

$$\text{If } T_{50}>510°C,\ \gamma_{gw} = 31+6872(O) \qquad \text{Eqn. 2}$$

$$\text{If } T_{50} \le 510°C,\ \gamma_{gw} = 241+15(Ni)^2-434(Mo) \qquad \text{Eqn. 3}$$

Where,

γ_{gw} = austenite grain width, microns,

dT/dt = calculated cooling rate at 538°C, °C /s, and

elements as designated in units of wt.%.

Strength Model

A single model for σ_y was determined. However, two models were necessary to describe σ_{uts}. The best fitting models for σ_{uts} were found when considering the range of expected T_{50}. One model best described the σ_{uts} when T_{50} was greater than 510°C, and another when T_{50} was less than or equal to 510°C. The strength model equations are given in Eqns. 4-6.

The σ_y correlated with T_{50}, grain width, and plate thickness. Cooling rate was also a factor in the σ_y equation, but it was incorporated in the T_{50} term, as will be shown in the "T_{50} Model" section. It was not entirely clear why plate thickness was a factor. Since it is related to cooling rate, it could have been a manifestation of cooling rate or a representation of weld bead size. Since cooling rate depends on bead size and plate thickness, the specification of both plate thickness and cooling rate essentially define the weld bead size or heat input which may be related to the reheating effect in multipass welds.

The σ_{uts} correlated with T_{50}, C, and cooling rate. The C*dT/dt term was highly significant in determining σ_{uts} when $T_{50} \le 510°C$. As was alluded to earlier in reference to Figure 8, σ_{uts} appeared to have a different dependence on T_{50}. Figure 16 indicates that another significant factor in addition to T_{50} in the development of σ_{uts} is the carbon content. Figure 16 is a plot of the prediction error when considering only T_{50} in the regression and data when T_{50} was $\le 510°C$. It shows that as carbon content increased, the correlation resulted in increasing under-prediction. Therefore, other terms such as carbon and cooling rate were considered in the regression analyses for σ_{uts} when $T_{50} \le 510°C$. The statistical analysis indicates that T_{50} had an effect on σ_{uts} for all values of T_{50}. But when $T_{50} \le 510°C$, C and dT/dt provided an additional effect to result in a steeper slope in Figure 8.

$$\sigma_y = 1297+14*z -1.2*T_{50} -0.48*\gamma_{gw} \qquad \text{Eqn. 4}$$

If $T_{50} \leq 510°C$, $\sigma_{uts} = 1332-1.38*T_{50}+61*C*dT/dt$ Eqn. 5

If $T_{50} > 510°C$, $\sigma_{uts} = 890-0.48*T_{50}$ Eqn. 6

Where,

σ_y = 0.2% offset yield strength, MPa,

σ_{uts} = ultimate tensile strength, MPa,

z = plate thickness, cm,

dT/dt = calculated cooling rate at 538°C, °C/s,

γ_{gw} = austenite grain width, microns and,

C = Carbon content, wt.%.

By substituting the calculated values for T_{50} (Eqn. 1) and γ_{gw} (Eqns. 2 & 3) into the strength models of Eqns. 4 through 6, σ_y and σ_{uts} can be calculated for a wide range of welding conditions based on expected weld deposit chemistry. Due to the dependence of these equations on the value of T_{50}, it is necessary to calculate T_{50} first and then proceed to the other equations. The overall fit of the model is demonstrated in Figure 17.

CVN Model

As described in the approach, a detailed statistical analysis was performed to determine the primary factors governing CVN impact toughness at –51°C. It was found that the most influencial variable affecting the CVN impact toughness was the σ_y/σ_{uts} ratio. This relationship is shown in Figure 18. A σ_y/σ_{uts} ratio of approximately 0.92 resulted in the peak toughness. The variables C*dT/dt, and Si/O were also significant variables in determining peak toughness performance, as shown in Figures 19 and 20. These variables, shown graphically in Figures 18 to 20, were incorporated into a regression analysis in addition to the σ_y/σ_{uts} ratio. The σ_y/σ_{uts} ratio, C*dT/dt, and Si/O terms all proved to be statistically significant. The result of the regression analysis is given in Eqn. 7. It should be noted that in addition to the σ_y/σ_{uts} ratio, C*dT/dt, and Si/O, that thickness and ln(dT/dt) were also significant variables in the regression analysis. Once again, as with strength, the combination of thickness and cooling rate may indicate a dependence of toughness on bead size and/or degree of reheatng. The model fit the data reasonably well as shown in Figure 21.

$$\ln CVN = -0.16t+0.47\ln(dT/dt)+3.8(\sigma_y/\sigma_{uts})+0.06(Si/O)-0.45(C*dT/dt) \quad \text{Eqn. 7}$$

Discussion

Empirical models have been developed for GMAW which predict the strength and toughness behavior of high-strength, low-carbon, alloy-steel weld metal from the weld metal composition and welding parameters. It was found that one equation was sufficient to describe σ_y. This expression incorporated terms for thickness (z), 50% transformation temperature (T_{50}), and prior austenite grain width(γ_{gw}). However, it was found that to describe γ_{gw}, two equations were necessary. One equation when the microstructure did not contain martensite, and one equation when the microstructure did contain martensite. In the case when the microstructure did not contain martensite, the γ_{gw} was dependent on weld metal oxygen content only. In the case when the microstructure contained martensite, γ_{gw} was dependent on weld metal Ni and Mo contents. In essence, two equations were

necessary to describe σ_y.

Two separate equations were necessary for describing σ_{uts}. These equations also depended on whether martensite was present. For non-martensitic structures, σ_{uts} depended solely upon T_{50}. For martensitic structures, σ_{uts} depended on weld metal C content and cooling rate in addition to T_{50}.

A model for T_{50} was also developed. This model incorporated terms for cooling rate, C, Ni, Mo, and Si/O ratio. This model was much different than any reported in the literature in that it included terms for cooling rate and oxygen content.

Since it was essential to know the microstructure type in order to apply the models, a means for describing the microstructure was essential. T_{50} was instrumental in providing such a means. It was found that when T_{50} was 510°C or less, the microstructure always contained some martensite. In the model developed in this work, a T_{50} of 510°C was the trigger point for the model to utilize the appropriate equations.

The effects of alloying on strength can be seen most clearly by reducing Eqns. 4-6 to their most basic forms as shown in Eqns. 8–11. Generally, the effect of alloying on strength was to increase strength in a linear fashion, except for Ni. Ni was the only element which suppressed T_{50} and increased grain size (if $T_{50} \leq 510°C$). Therefore, the overall effect of Ni was not linear. The effect of Ni on strength was parabolic in nature with the maxima occurring when T_{50} was equal to 510°C. Therefore, the effect of Ni on strength, when $T_{50} > 510°C$, was to increase strength. When $T_{50} \leq 510°C$, the effect of Ni was to decrease strength.

$$\text{If } T_{50} \leq 510°C,\ \sigma_y = 245+14t+16\ln dT/dt+1519C+54Ni-7Ni^2+275Mo+4.3Si/O \quad \text{Eqn. 8}$$

$$\text{If } T_{50} \leq 510°C,\ \sigma_{uts} = 256+18\ln dT/dt+1747C+61C*dT/dt+77Mo+62Ni+5Si/O \quad \text{Eqn. 9}$$

$$\text{If } T_{50} > 510°C,\ \sigma_y = 346+14t+16\ln dT/dt+1519C+67Mo+54Ni+4.3Si/O-3300(O) \quad \text{Eqn. 10}$$

$$\text{If } T_{50} > 510°C,\ \sigma_{uts} = 516+6\ln dT/dt+608C+27Mo+22Ni+1.7Si/O \quad \text{Eqn. 11}$$

The factors found to be significant in the development of CVN toughness at –51°C were z, $\ln dT/dt$, σ_y/σ_{uts} ratio, C*dT/dt, and Si/O. Although it was shown that the terms σ_y/σ_{uts} ratio, C*dT/dt, and Si/O displayed optimum toughness at specific values, the final model indicates that the optimum ratios will depend on the remaining alloy chemistry. This creates difficulty in weld metal design when trying to achieve optimum properties over a wide range of operating conditions since changing weld parameters affect chemistry and cooling rate.

The maximum toughness generally occurred when T_{50} was equal to 510°C. This was when martensite began to emerge in the microstructure. This suggests that a small amount of martensite is desirable in the microstructure.

The effects of alloying on toughness is not as clear as its effects on strength due to the existence of variables which reside in both the numerator and denominator. However, the following analysis is provided to simplify the matter. Since the σ_y/σ_{uts} ratio is the primary factor in determining the toughness, it will be the focus of the discussion. Eqns. 8-11 contain sets of variables for σ_y and σ_{uts}. Thus analyzing the difference between these two sets and the ratios of each common coefficient for each case when $T_{50} > 510°C$ and when $T_{50} \leq 510°C$ reveals which variables have the largest effect on the σ_y/σ_{uts} ratio for a given alloy system. When $T_{50} > 510°C$ the difference between the sets of variables for σ_y and σ_{uts} is the terms z(+), and O(-) in the numerator. The (+) and (-) indicates the sign of the coefficient. This indicates that thickness and oxygen have a strong effect on the σ_y/σ_{uts} ratio. Increasing thickness and decreasing oxygen content increased the ratio and hence the toughness. The common terms were $\ln dT/dt$, C, Mo, Ni, and Si/O. The ratio of coefficients for common terms ranged from 2.0 to 2.7. A ratio greater than 1 indicates that the term has the effect of increasing the σ_y/σ_{uts} ratio and hence the toughness when $T_{50} > 510°C$. Therefore, increasing dT/dt, C,

Mo, Ni, and Si/O also increased the σ_y/σ_{uts} ratio and the toughness.

When $T_{50} \leq 510°C$ the difference between the sets of variables for σ_y and σ_{uts} is the terms z(+), and Ni^2(-) in the numerator, and C*dT/dt(+) in the denominator. This indicates that terms z, and Ni^2 have a strong effect on the σ_y/σ_{uts} ratio. Increasing z and decreasing C*dT/dt and Ni contents tended to increase the ratio and hence the toughness. The common terms were lndT/dt, C, Mo, Ni, and Si/O. The ratio of coefficients for common terms ranged from 0.8 to 0.9. A ratio of less than 1 indicates that the term has the effect of decreasing the σ_y/σ_{uts} ratio and hence the toughness when $T_{50} \leq 510°C$. Therefore, increasing dT/dt, C, Mo, Ni, and Si/O also tends to decrease the σ_y/σ_{uts} ratio and the toughness.

Optimized Compositions

The data presented in this report is only a small portion of the total data which was developed throughout the wire development program. Upon considering the total data an optimized wire composition was specified as shown in Table 2. This wire is currently in production.

Although the final composition evolved from the total data set, the model described herein was also used to determine the optimum weld deposit composition. This was done by generating a factorial designed experiment and executing the model. The factors used in the model were cooling rate, C, Ni, Mo, Si, and O. The factors were varied within the range of actual experimentation. The selection of the best compositions were done so at slow cooling rate conditions (3°C/s and 5.5°C/s). The optimum compositions from the slow cooling rate conditions were then analyzed to evaluate a fast cooling rate condition (61°F/s). The toughness requirement to be met at these conditions was 47 joules at –51°C. The strength requirements were 566 MPa minimum yield strength at 3°C/s and 607 MPa at 5.5°C/s. The goal was to find a single composition meeting all of these requirements.

When determining the optimum compositions, it was necessary to address the following items: (1) the model does not incorporate Mn, Al, or Ti contents. However, it is believed that they play an important role in determining the final weld deposit oxygen content. In determining the optimum compositions, the Mn, Al, and Ti contents were therefore fixed, but the oxygen level allowed to vary, and (2) the experimental wires leading up to the production heat were vacuum degassed and therefore their deposits displayed low oxygen values near 200 ppm. It is likely that in the absence of vacuum degassing that an increase in wire oxygen will be experienced and possibly an increase in the deposit oxygen content. Therefore, optimum compositions were determined for oxygen values of 200 and 250ppm to account for this possible increase.

The results of the model optimization process are shown in Table 3. Considering elemental gains and losses during the welding process, the deposit compositions of Table 3 are remarkably similar to that of Table 2. The total data set showed that there was minimal gains and losses in Mo and Ni. Therefore, the Mo and Ni contents of the deposit are expected to be similar to that of the wire composition. It also showed that the C content of the deposit was higher than the wire composition by 0.01% to 0.02% when using $C0_2$ shielding gas mixtures. Therefore, it is likely that the deposit will contain up to 0.04% C. The data also showed that the weld deposit silicon content could be either higher or lower than the original wire composition. Therefore, it is likely that the deposit silicon content will vary from about 0.30% to 0.40 %.

Two compositions are shown in Table 3. The predicted optimum composition was a function of the oxygen content. It is shown that for an increase in oxygen from 200ppm to 250 ppm that a corresponding increase in Ni from 2.4 to 2.6 was required. It is not likely that that these compositions will be maintained over a large range of welding parameters and changing base plate materials. However, a single weld wire composition was desirable to satisfy all conditions.

Table 2. Specified Weld Wire Composition

Element	Aim	Range
C	0.020	0.025 Max.
Mn	1.90	1.80-2.00
Mo	0.60	0.55-0.65
Ni	2.60	2.50-2.70
Si	0.35	0.30-0.40
Cr	LAP*	0.15 max.
P	LAP	0.008 max.
S	0.002 max.	0.005 max.
Cu	LAP	0.15 max.
V	LAP	0.25 max.
Ti	0.015	0.010-0.020
Al	LAP	0.010 max.
B	LAP	0.001 max.
N	LAP	0.008 max.
O	LAP	0.005 max.
H	LAP	<0.0002
Nb	LAP	0.005 max.
Zn, As, Zr, Sn, Sb, Ta, Pb, Bi	LAP	0.025 max.
W	LAP	0.035 max.
Ca	LAP	0.0020 max.

* Low as possible.

Table 3. Predicted Optimum Weld Deposit Compositions

O	C	Mo	Ni	Si
0.02	0.04	0.6	2.4	0.4
0.025	0.04	0.6	2.6	0.4

A given wire composition will result in various deposit compositions depending on cooling rate, baseplate type, dilution, etc. The model shows that for a given cooling rate a unique composition exists which provides the best combination of strength and toughness. Therefore, it is not possible to achieve maximum toughness and optimum strength across a wide range of cooling rates when using a single wire composition. However, it is possible to optimize the composition of the welding wire to achieve acceptable properties over a range of cooling rates.

Summary

This report details a metallurgical analysis which identifies the factors affecting the strength and toughness behavior of newly developed low carbon welding consumables. It was found that the 50% transformation temperature (T_{50}) was a good indicator of the microstructure type and was successfully correlated to weld deposit strength. When $T_{50} \leq 510°C$, it was found that the microstructure contained some martensite. When $T_{50} > 510°C$, the microstructure did not contain martensite. Other factors responsible for strength development were prior austenite grain width

(γ_{gw}), cooling rate, multipass reheating, carbon content and oxygen.

Similarly, when describing the γ_{gw} it was found that it was dependent on the microstructure type. In the case when the microstructure did not contain martensite, the γ_{gw} was dependent on weld metal oxygen content only. In the case when the microstructure contained martensite, γ_{gw} was dependent on weld metal Ni and Mo contents.

The factors responsible for toughness development (@-51°C) were the yield to ultimate strength ratio, cooling rate, oxygen and carbon contents. The austenite grain width and 50% transformation temperature were modeled from welding parameters and weld deposit composition, permitting successful prediction of weld metal strength and toughness.

The model indicated that the optimum weld deposit chemistry to satisfy the strength requirements for both 566 MPa and 607 MPa applications is dependent upon the weld deposit oxygen content. It was found that the Ni content had to increase with corresponding increases in oxygen content. If the weld deposit oxygen content was expected to be 200ppm then the optimum weld deposit chemistry as predicted by the model was 0.04%C, 0.60% Mo, 2.4%Ni, and 0.4% Si. If the weld deposit oxygen content was expected to be 250ppm then the optimum weld deposit chemistry as predicted by the model was 0.04%C, 0.60% Mo, 2.6%Ni, and 0.4% Si.

References

[1] J. J. Deloach, *Welding and Weld Automation in Shipbuilding*, 85-104, TMS, Warrendale, PA (1996)
[2] F.B. Pickering, *Proceedings of Micro-Alloying 75*, 9-31, Union Carbide Corp., New York, NY (1977)
[3] D.Rosenthal, *Weld J.*, Res. Supp., 20(5), 220s-225s (1941)
[4] K. E. Dorschu, *Weld J.*, Res. Supp., 47(2), 49s-62s (1968)
[5] P. Jhaveri, W.G. Moffatt, and C.M. Adams, Jr, *Weld. J.*, Res. Supp., 41(1), 12-s to 16-s (1962)
[6] Irvine and Pickering, JISI, 193, 110-125 (1965)
[7] W. Steven, and A.O. Haynes, *JISI*, 183(8), 349-359 (1956)
[8] K.W. Andrews, *JISI*, 192(7), 721-727 (1965)

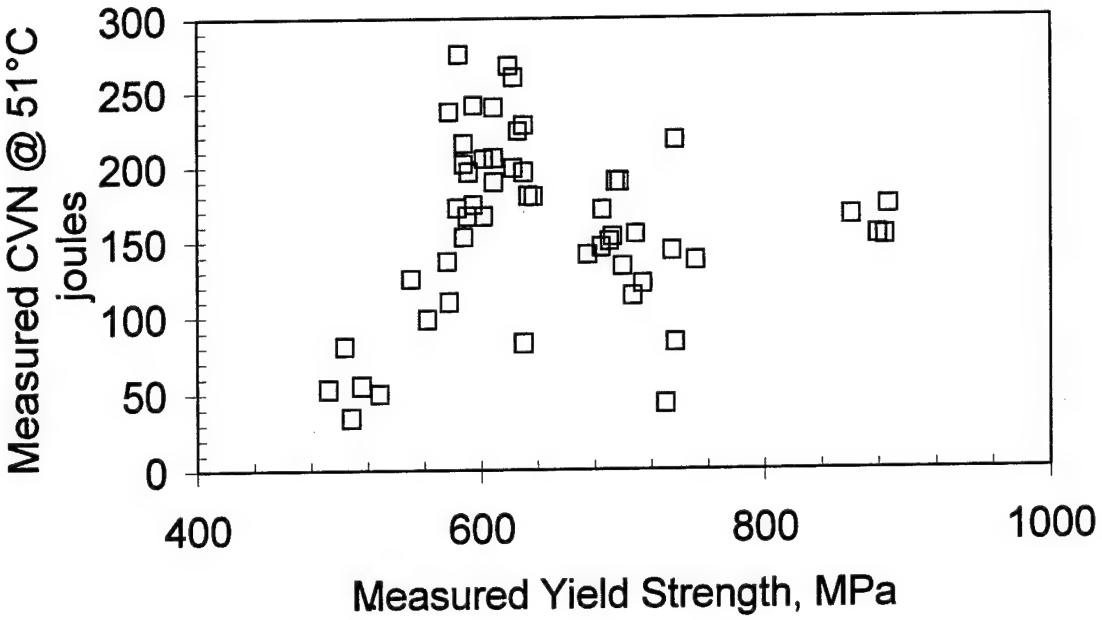

Figure 1. Relationship between strength and toughness.

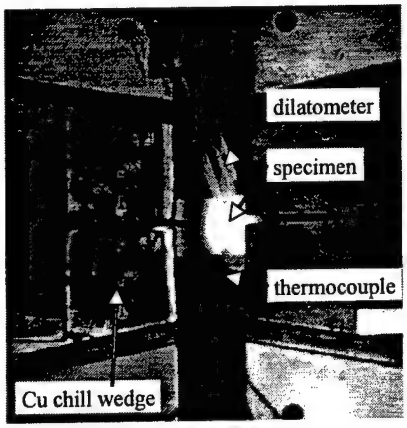

Figure 2. Gleeble dilatometer specimen during thermal cycling.

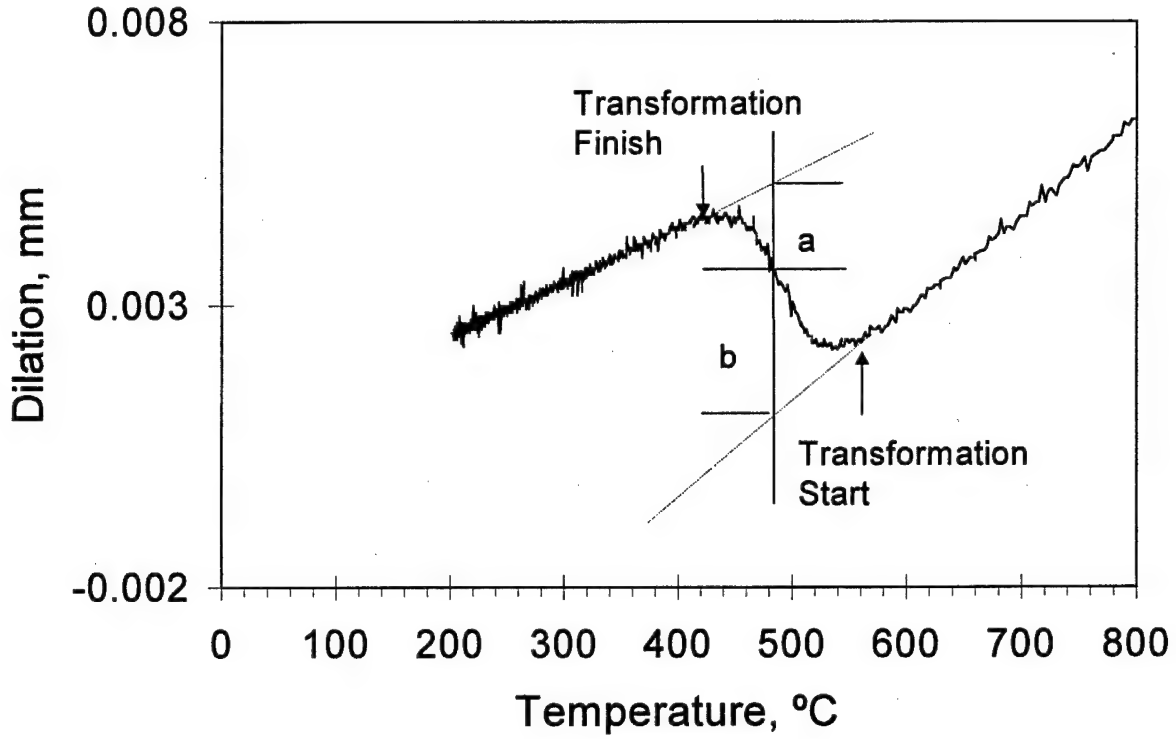

Figure 3. Dilatometry data analysis.

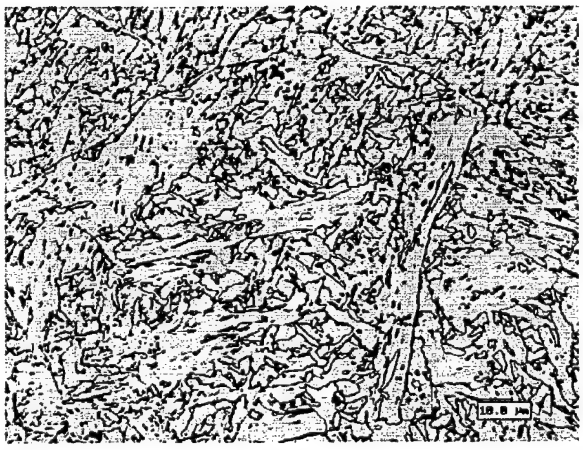

Figure 4. Photomicrograph of as-deposited weld metal deposited at a calculated cooling rate of 1°C/s. (ID# PD21222, T_{50}=590°C, Hv=208)

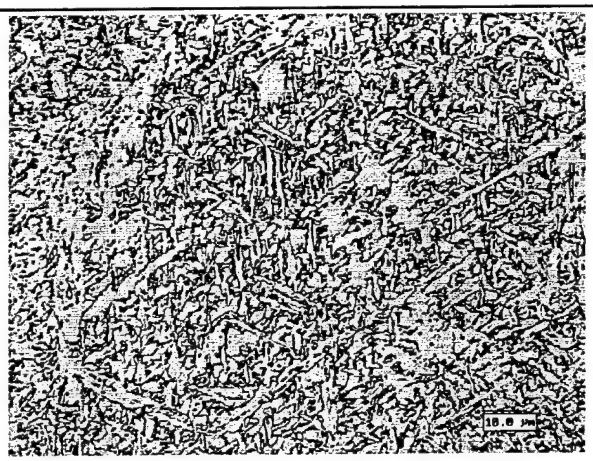

Figure 5. Photomicrograph of as-deposited weld metal deposited at a calculated cooling rate of 20°C/s. (ID# PD21278, T_{50}=510°C, Hv=257)

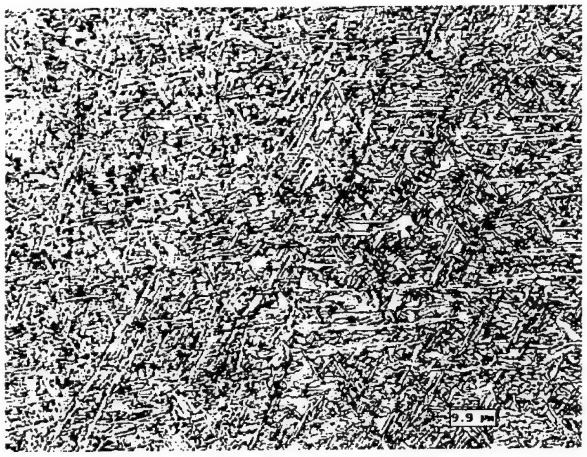

Figure 6. Photomicrograph of as-deposited weld metal deposited at a calculated cooling rate of 60°C/s. (ID# PD21251,T_{50}=420°C, Hv=316)

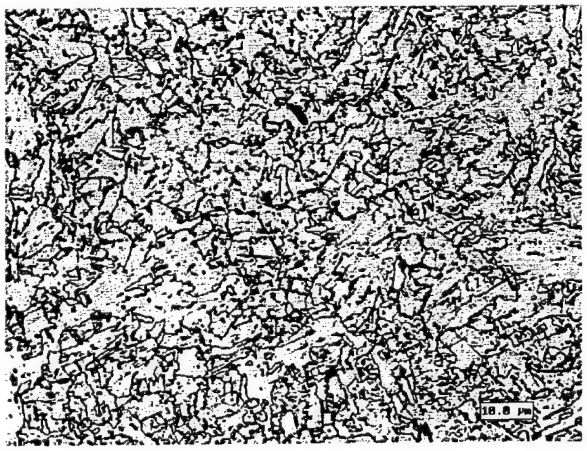

Figure 7. Photomicrograph of reheated weld metal originally deposited at a calculated cooling rate of 20°C/s. (ID# PD21278)

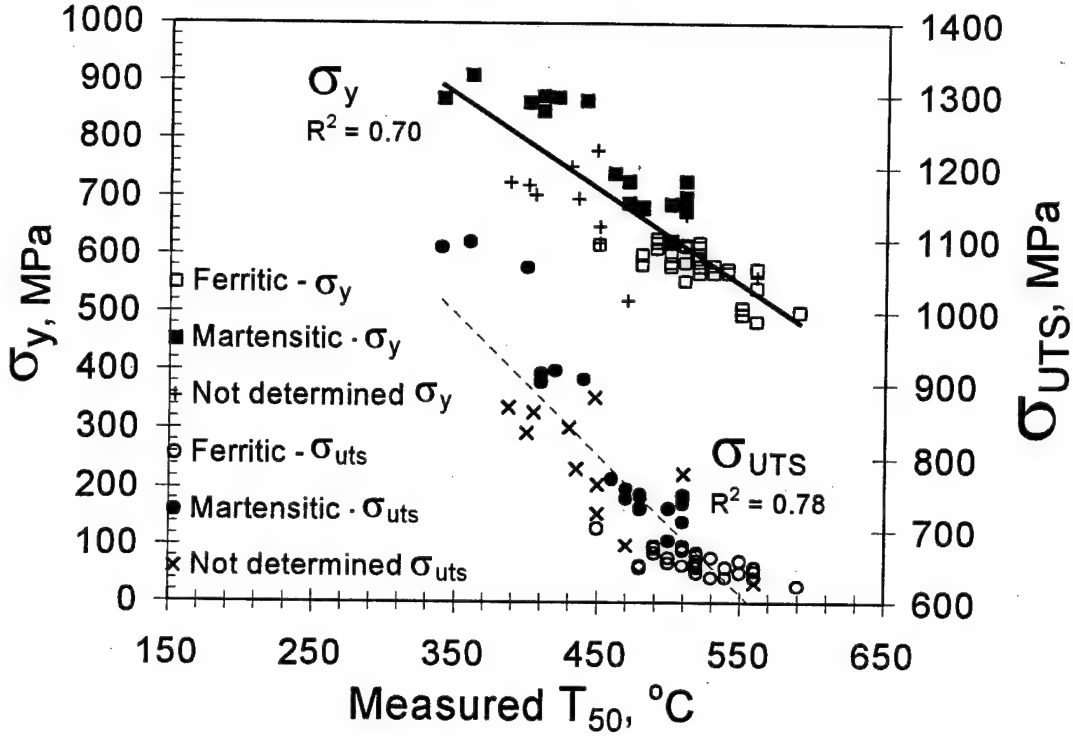

Figure 8. σ_y as a function of T_{50}.

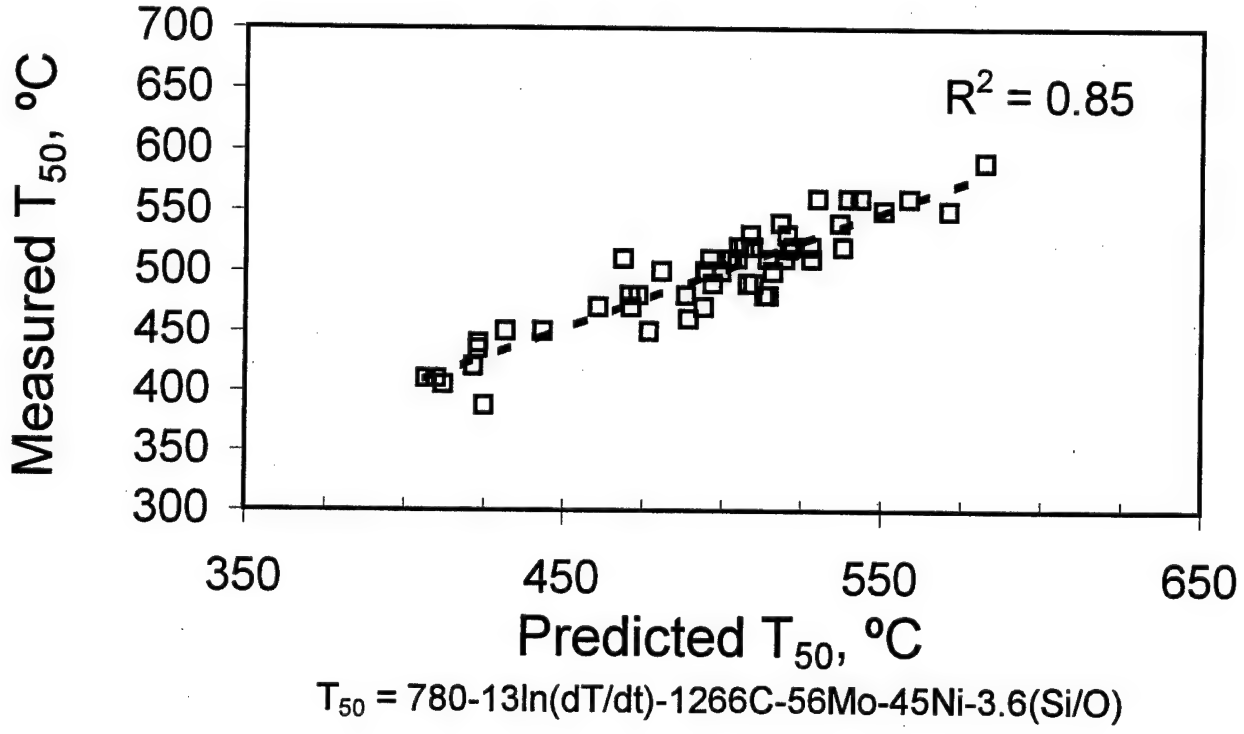

Figure 9. 50% transformation model.

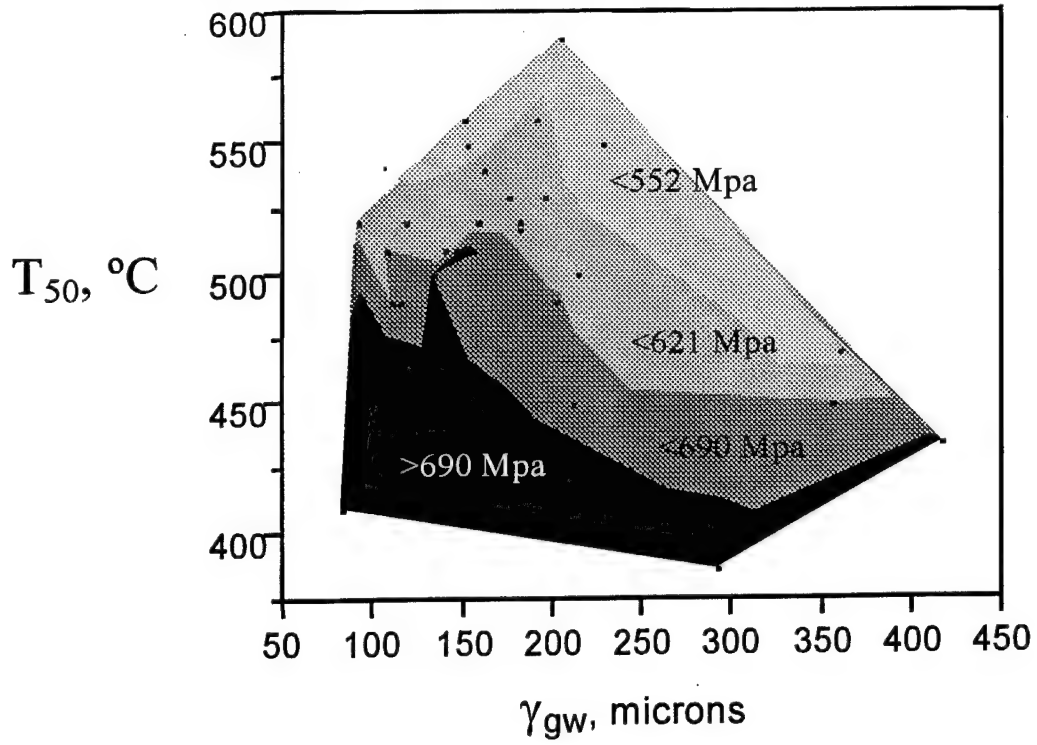

Figure 10. The effects of γ_{gw} and T_{50} on σ_y.

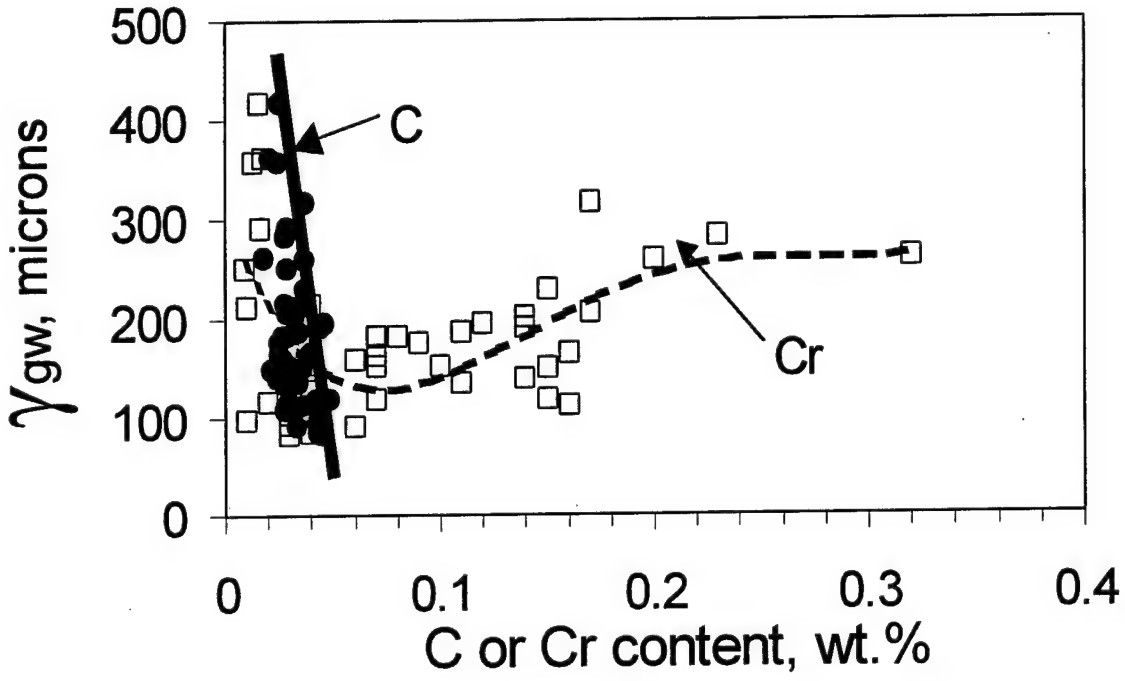

Figure 11. The effect of C and Cr on γ_{gw}.

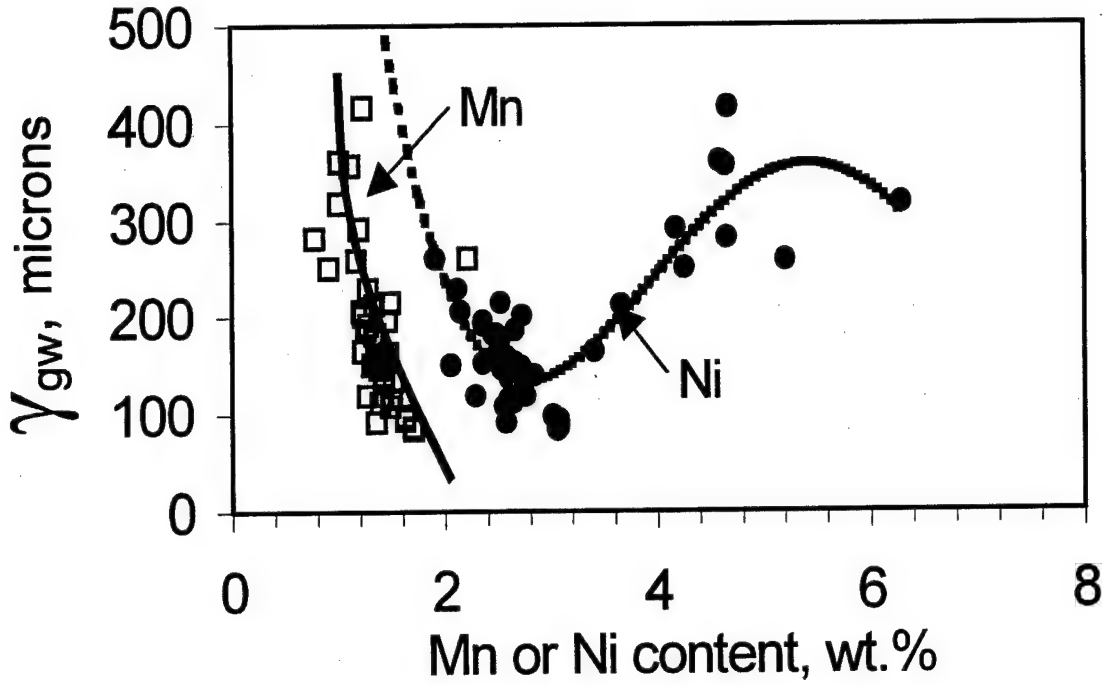

Figure 12. The effect of Mn and Ni on γ_{gw}.

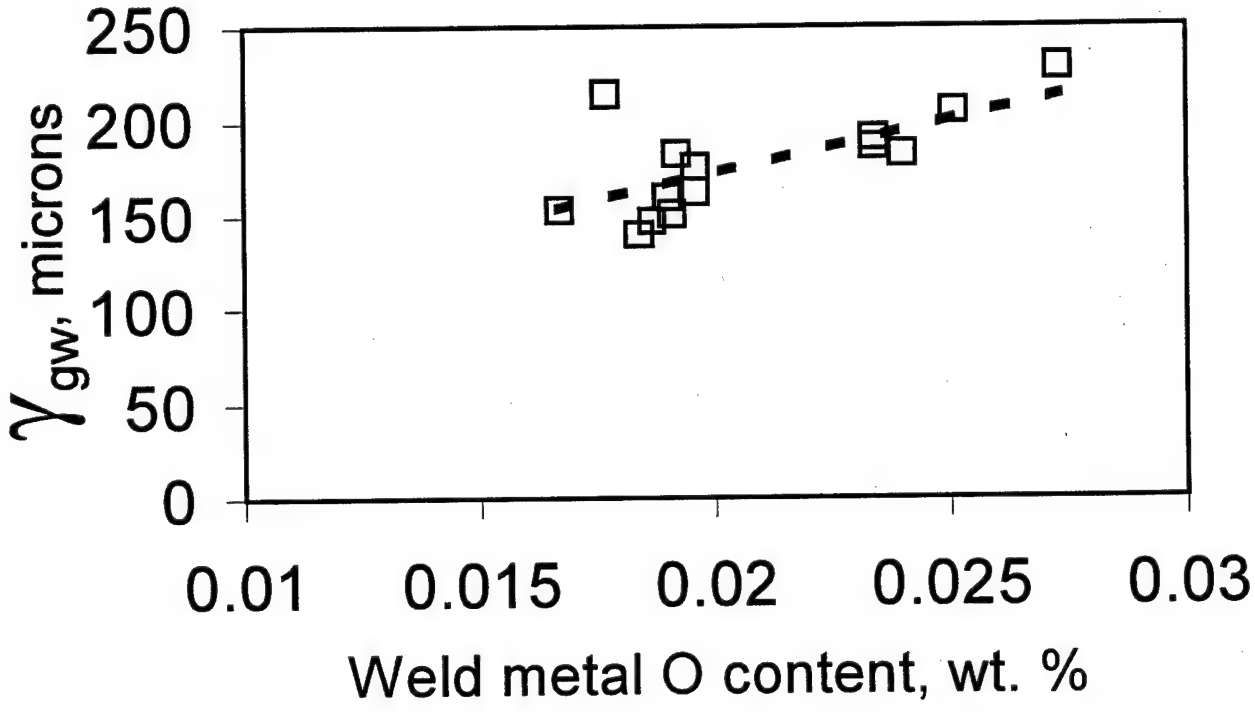

Figure 13. The effect of oxygen on γ_{gw} when T_{50}>510°C.

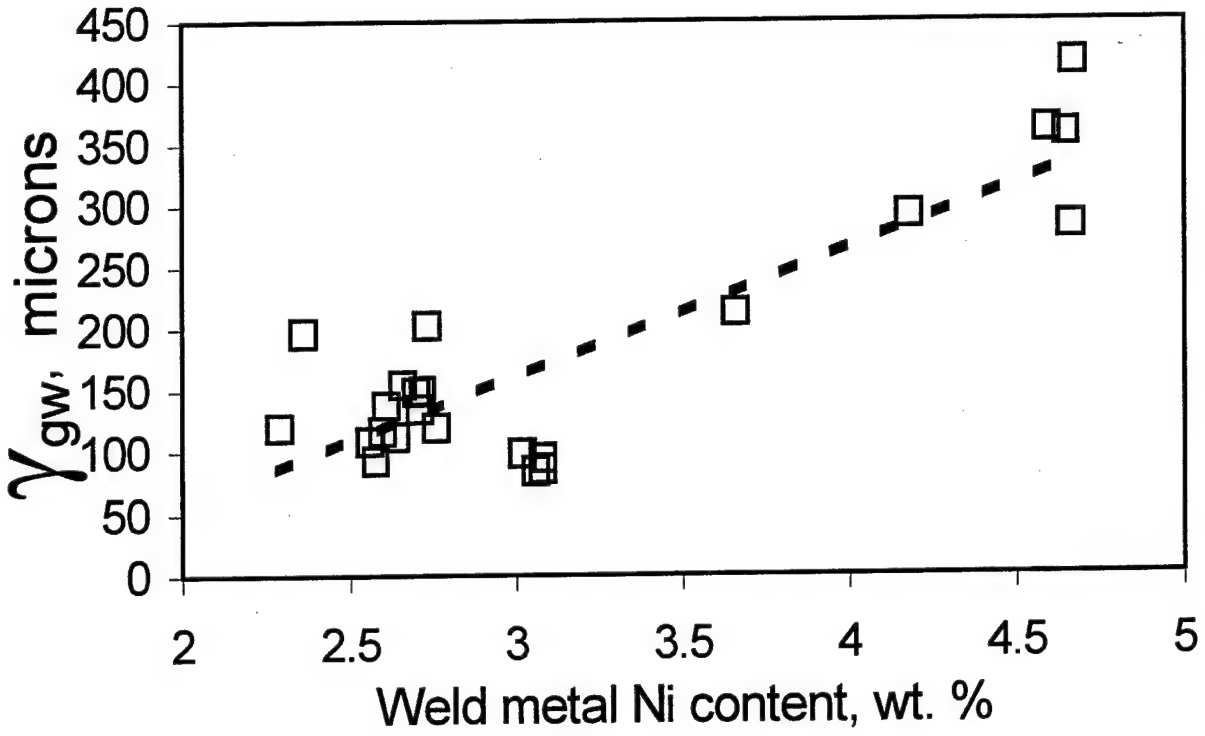

Figure 14. The effect of nickel on γ_{gw} when $T_{50} \leq 510°C$.

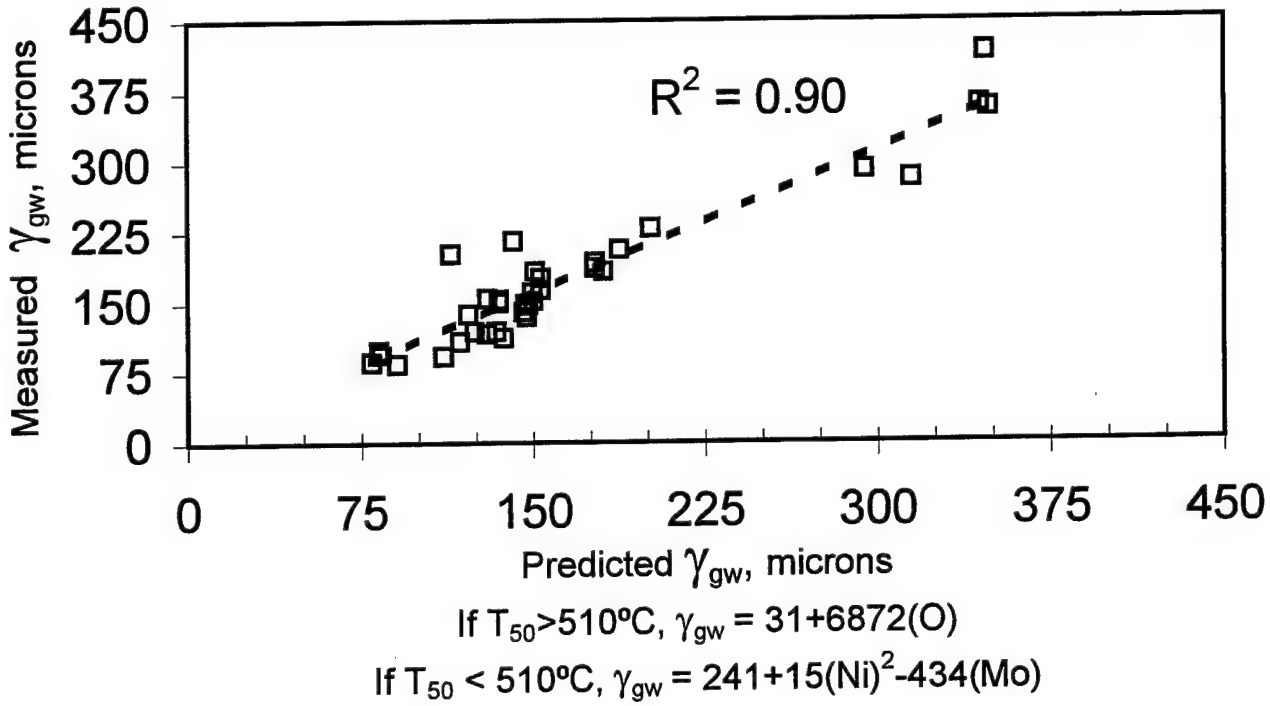

Figure 15. γ_{gw} prediction.

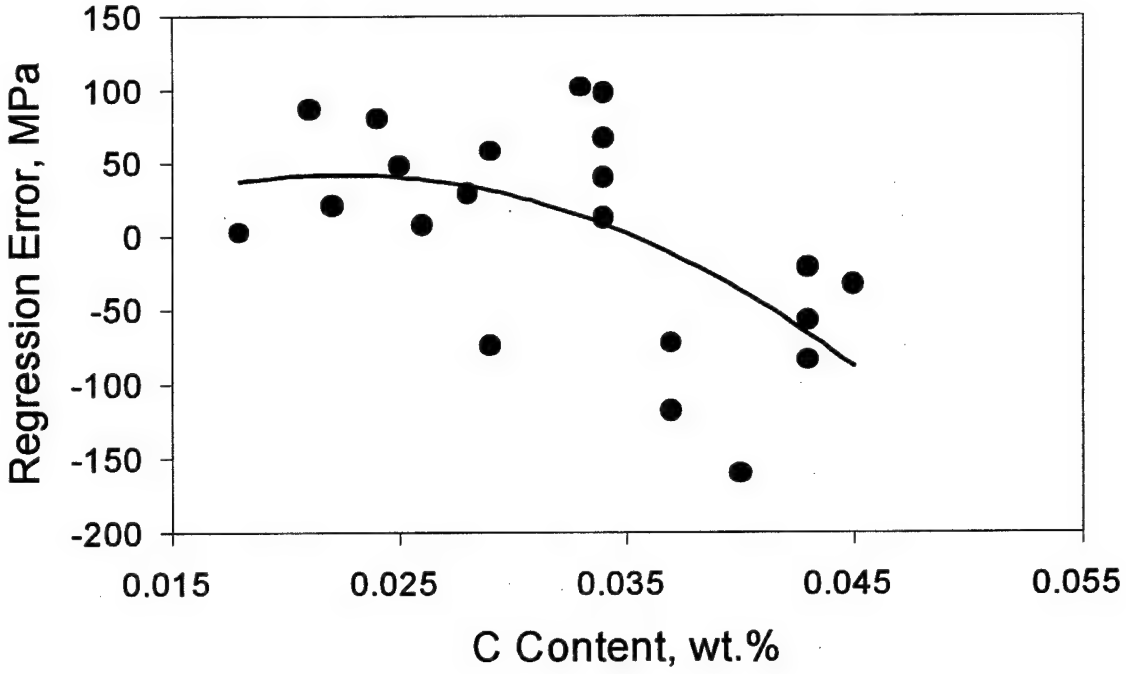

Figure 16. The significance of carbon content on strength development when $T_{50} \leq 510°C$.

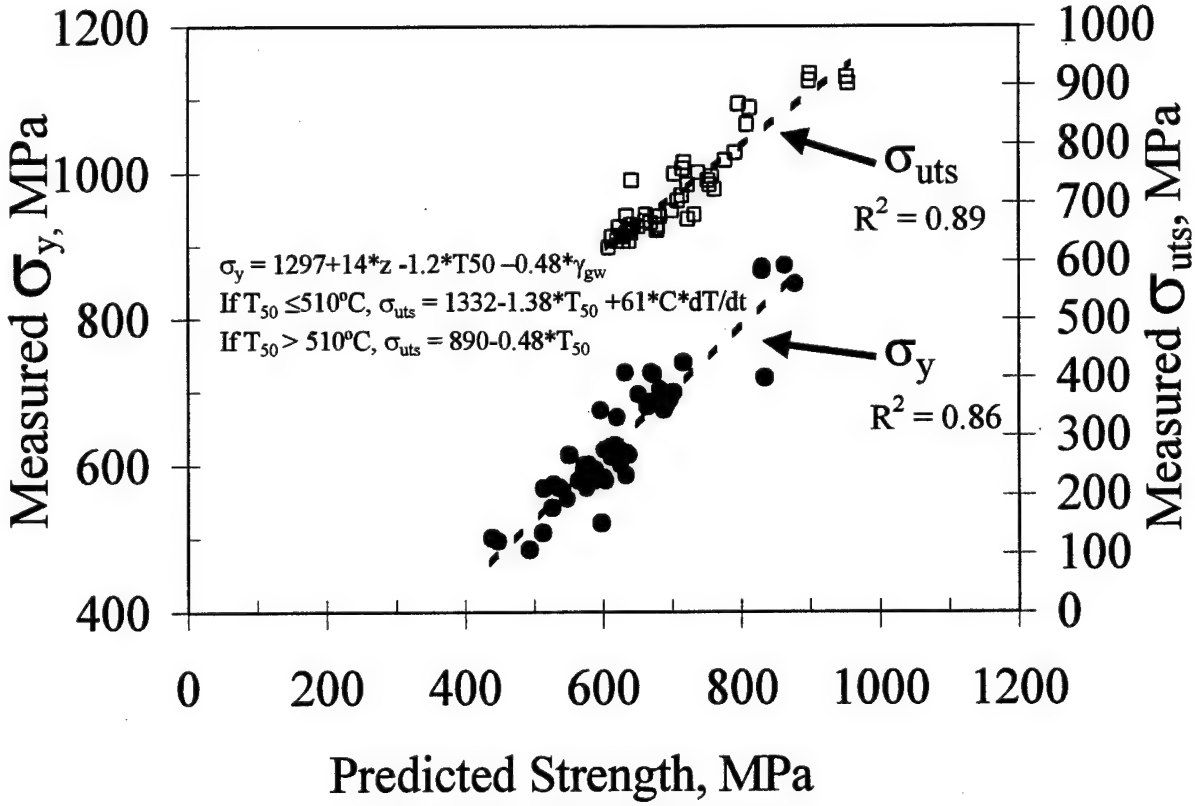

Figure 17. Strength predictions.

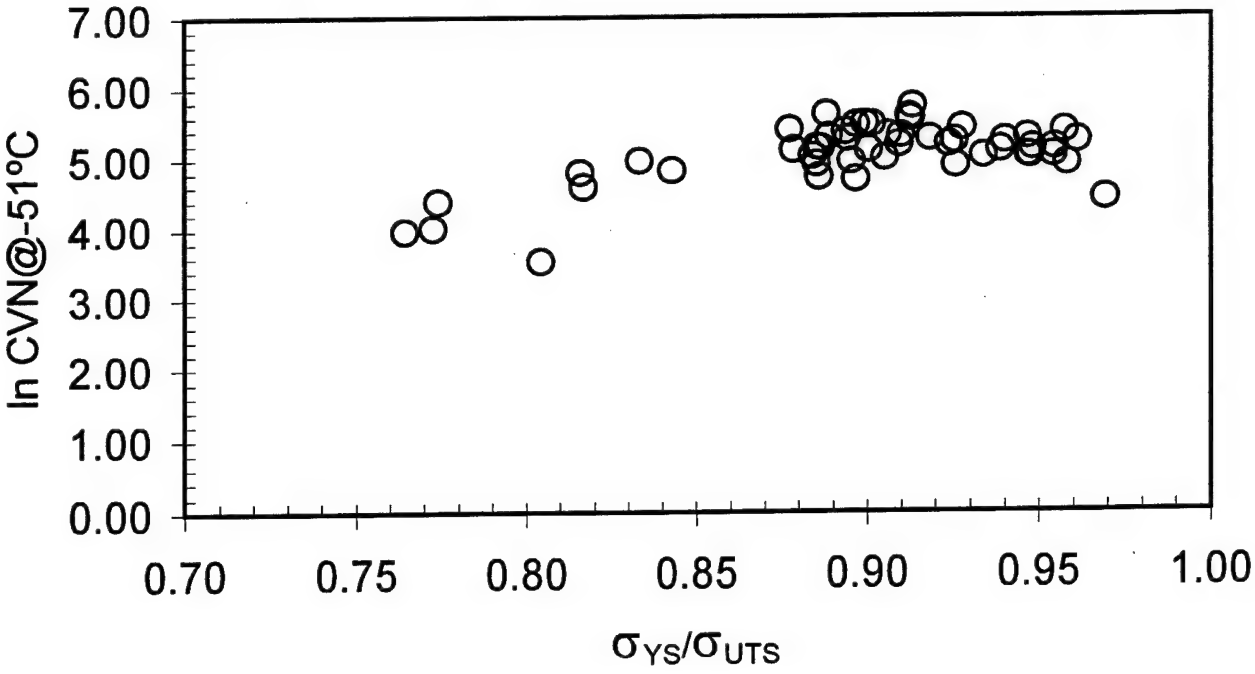

Figure 18. The influence of the σ_y / σ_{uts} ratio on weld metal toughness.

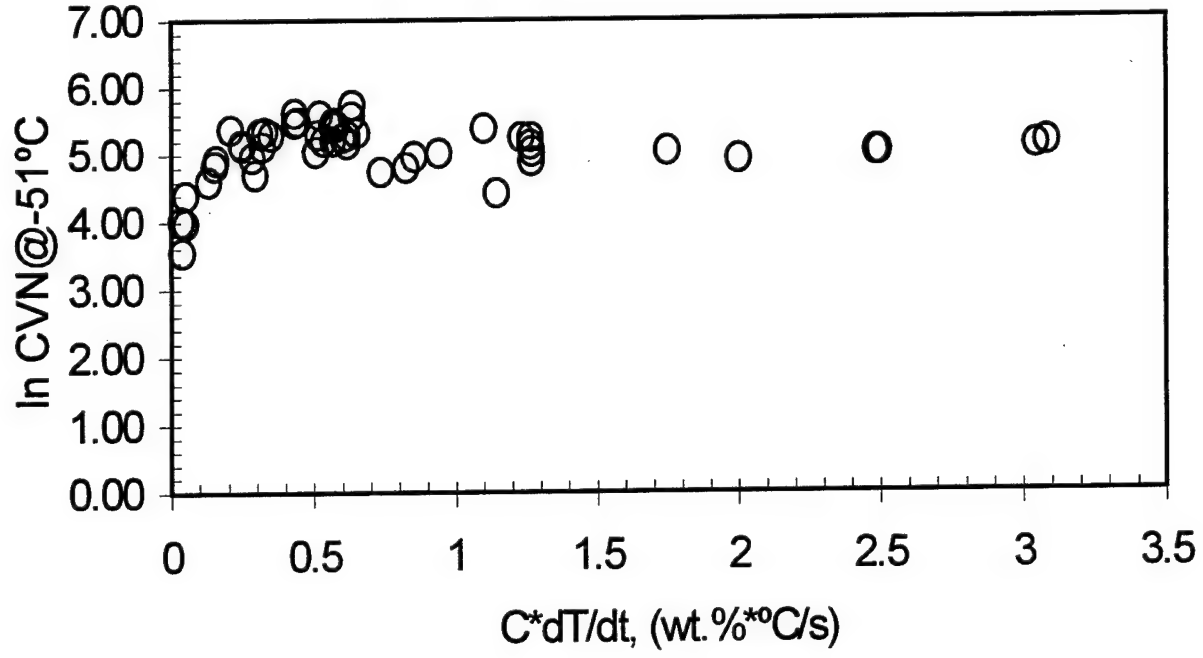

Figure 19. The influence of carbon content and cooling rate on weld metal toughness.

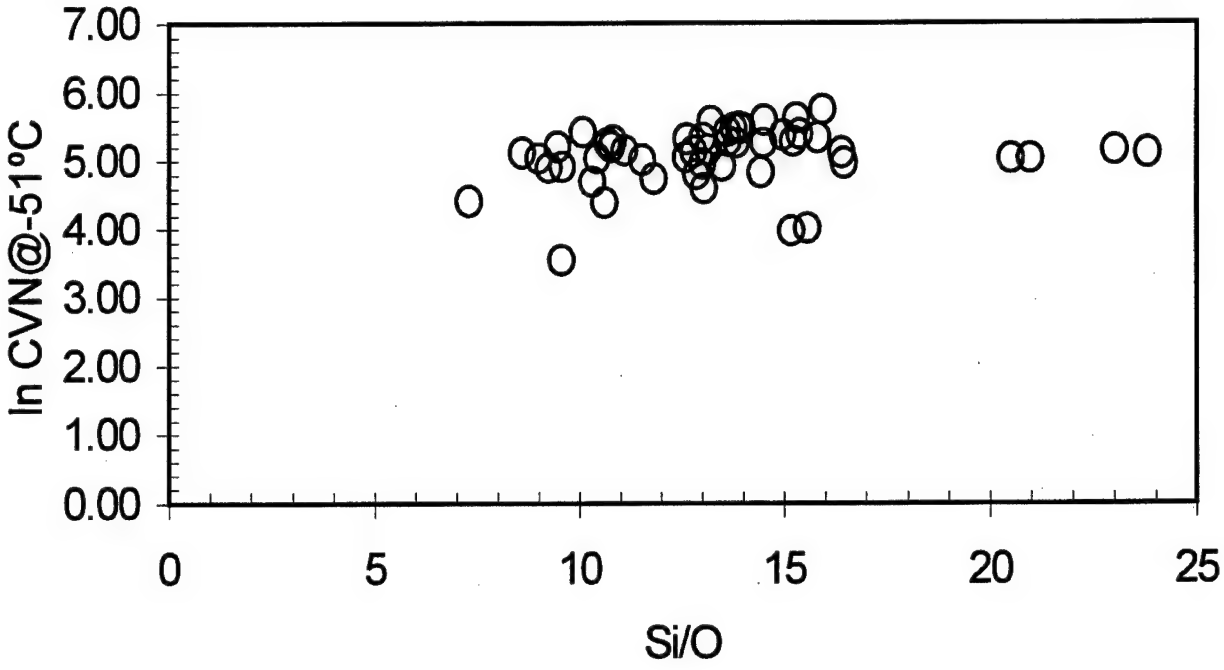

Figure 20. The influence of Si/O ratio on weld metal toughness.

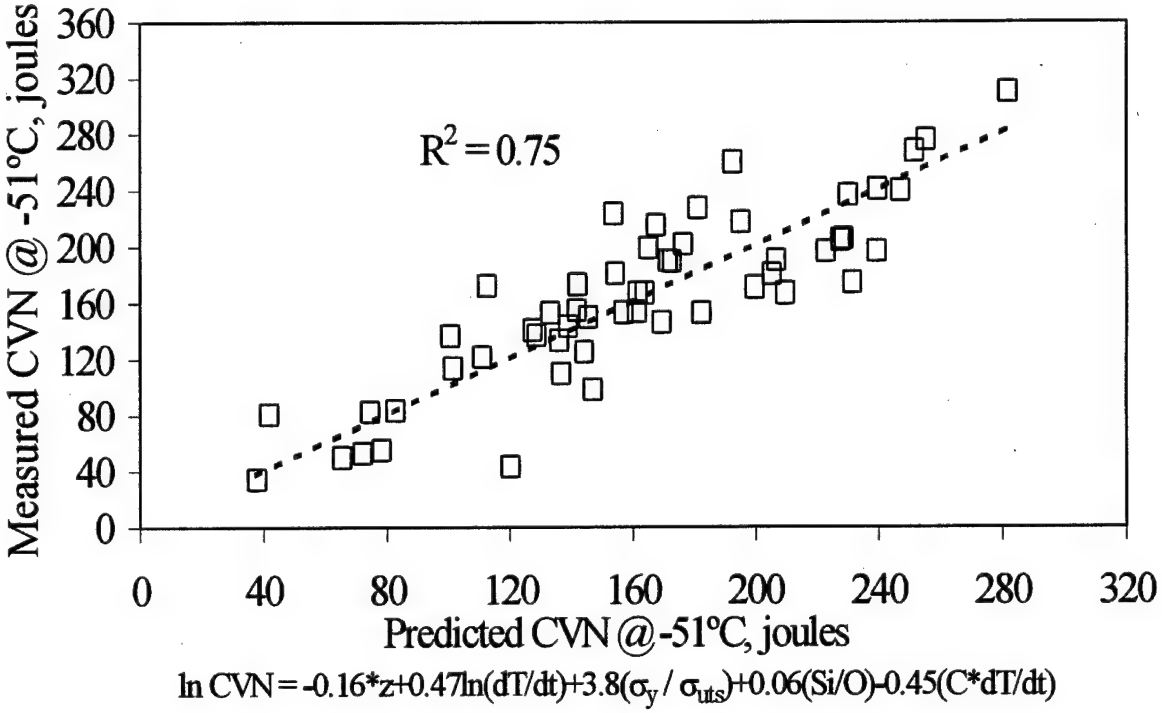

Figure 21. Correlation between predicted values of CVN @ -51°C and measured values.

Appendix 1- Weld metal chemistries, 50% transformation temperatures and prior austenite grain width

WELD ID	C wt. %	Mn wt. %	Si wt. %	Cr wt. %	Ni wt. %	Mo wt. %	Cu wt. %	S wt. %	P wt. %	Al wt. %	Ti wt. %	O wt. %	N wt. %	T_{50} °C	γ_{GS} µm
JB-32	0.025	1.23	0.26	0.02	4.67	0.51	0.16	0.002	<.004	0.003	0.009	0.022	0.002	435	416
JB-33	0.024	1.11	0.18	0.01	4.65	0.50	0.19	0.002	<.004	0.002	0.005	0.026	0.004	450	357
JB-34	0.021	1.01	0.19	0.02	4.59	0.49	0.30	0.003	0.19	0.003	0.008	0.047	0.004	470	361
JB-37	0.034	1.34	0.28	0.01	3.66	0.44	0.21	0.002	0.003	0.002	0.008	0.014	0.003	450	212
MV-10	0.029	0.91	0.14	0.01	4.3	1.33	0.22	0.003	0.003	0.007	0.002	0.036	0.009	448	251
MV-13	0.028	0.78	0.27	0.23	4.7	0.58	0.16	0.005	0.003	0.0024	0.009	0.021	0.0008	405	282
MV-14	0.029	1.20	0.28	0.02	4.2	0.48	0.18	0.005	0.006	0.0032	0.010	0.017	0.0004	387	292
PD21080	0.038	1.31	0.28	0.16	2.64	0.49	0.013	0.002	0.001	0.006	0.007	0.0187	0.0013	520	
PD21081 S1	0.034	1.43	0.29	0.11	2.61	0.51	0.008	0.002	0.002	0.008	0.004	0.0215	0.0018	460	137
PD21081 S2	0.03	1.43	0.27	0.07	2.66	0.5	0.003	0.001	0.001	0.008	0.004	0.0214	0.0009	510	154
PD21092 S1	0.026	1.52	0.28	0.04	2.71	0.48	0.075	0.001	0.002	0.002	0.005	0.0182	0.0032	470	
PD21092 S2	0.028	1.52	0.29	0.04	2.71	0.47	0.108	0.001	0.003	0.003	0.005	0.02	0.0013	500	134
PD21149	0.049	1.27	0.29	0.15	2.29	0.45	0.13	0.003	0.003	0.011	0.004	0.0213	0.0058	520	119
PD21150	0.037	1.28	0.29	0.15	2.12	0.43	0.13	0.005	0.003	0.002	0.004	0.0273	0.0032	550	229
PD21151 S1	0.022	1.4	0.27	0.04	2.7	0.47	0.078	0.001	0.003	0.003	0.004	0.0195	0.0018	510	148
PD21151 S2	0.022	1.41	0.27	0.03	2.72	0.5	0.091	0.001	0.002	0.002	0.004	0.0211	0.0023	510	149
PD21171	0.036	1.31	0.29	0.15	2.06	0.42	0.25	0.002	0.006	0.006	0.004	0.0191	0.0029	560	151
PD21172	0.028	1.49	0.28	0.04	2.53	0.46	0.093	0.001	0.002	0.005	0.004	0.0177	0.0019	500	215
PD21175	0.03	1.51	0.27	0.02	2.6	0.49	0.051	0.001	0.002	0.0047	0.005	0.0186	0.0056	490	116
PD21176	0.044	1.28	0.26	0.14	2.36	0.46	0.235	0.002	0.003	0.001	0.004	0.0234	0.0034	560	192
PD21177	0.034	1.26	0.25	0.11	2.66	0.48	0.014	0.002	0.003	0.003	0.003	0.0234	0.0034	480	187
PD21178	0.036	1.39	0.28	0.16	2.64	0.48	0.005	0.001	0.003	0.003	0.004	0.0184	0.0021	490	112
PD21202	0.029	1.33	0.26	0.08	2.48	0.49	0.17	0.002	0.003	0.01	0.004	0.024	0.003	520	183
PD21215	0.027	1.36	0.24	0.06	2.58	0.54	0.098	0.002	0.001	0.011	0.006	0.019	0.0022	520	160
PD21216	0.033	1.36	0.25	0.06	2.58	0.53	0.084	0.003	0.002	0.009	0.006	0.0179	0.0063	520	92
PD21217	0.025	1.26	0.22	0.09	2.5	0.53	0.123	<0.001	0.002	0.008	0.005	0.0213	0.002	540	
PD21220	0.028	1.25	0.23	0.17	2.79	0.43	0.28	0.004	0.003	0.003	0.006	0.024	0.0026	520	
PD21222	0.029	1.22	0.24	0.17	2.15	0.46	0.256	0.005	0.003	0.001	0.006	0.0251	0.0032	590	206
PD21232	0.03	1.36	0.2	0.11	3.58	0.51	0.008	0.003	0.001	0.006	0.006	0.0211	0.0016	500	
PD21233	0.033	1.47	0.22	0.09	3.55	0.5	0.006	0.002	0.001	0.004	0.008	0.0218	0.0016	450	
PD21234	0.032	1.23	0.23	0.14	2.73	0.55	0.008	0.003	0.002	0.009	0.005	0.0213	0.007	490	202
PD21235	0.035	1.31	0.25	0.14	2.68	0.55	0.004	0.002	0.003	0.006	0.006	0.019	0.0021	500	
PD21242	0.027	1.35	0.25	0.07	2.45	0.47	0.111	0.003	0.002	0.005	0.003	0.0192	0.0011	518	183
PD21243	0.021	1.38	0.19	0.05	3.41	0.47	0.096	0.001	0.002	0.004	0.006	0.0182	0.0007	500	
PD21251 S1	0.043	1.63	0.34	0.01	3.02	0.68	0.1	0.004	0.003	0.005	0.009	0.0162	0.0016	440	98
PD21251 S2	0.043	1.63	0.32	0.03	3.08	0.69	0.146	0.002	0.003	0.006	0.01	0.0156	0.0022	420	94
PD21252 S2	0.022	1.51	0.21	0.03	3.63	0.49	0.114	0.001	0.003	0.01	0.008	0.0182	0.0013	480	

Appendix 1 (cont'd)

WELD ID	C	Mn	Si	Cr	Ni	Mo	Cu	S	P	Al	Ti	O	N	T_{50}	γ_{GS}
	wt. %	wt. %	wt. %	wt. %	wt. %	wt. %	wt. %	wt. %	wt. %	wt. %	wt. %	wt. %	wt. %	°C	μm
PD21253 S1	0.022	1.46	0.2	0.02	3.65	0.52	0.068	0.004	0.002	0.001	0.007	0.0222	0.0011	480	
PD21253 S2	0.022	1.47	0.2	0.03	3.67	0.53	0.114	0.003	0.002	0.001	0.007	0.0216	0.0012	470	
PD21254 S1	0.045	1.71	0.35	0.03	3.06	0.67	0.142	0.001	0.005	0.006	0.012	0.0152	0.0012	410	84
PD21254 S2	0.043	1.7	0.35	0.04	3.08	0.7	0.128	0.003	0.003	0.013	0.012	0.0147	0.001	410	86
PD21255	0.025	1.38	0.26	0.03	2.54	0.48	0.081	0.002	0.001	0.001	0.003	0.0187	0.0011	510	147
PD21256	0.018	1.4	0.18	0.04	3.46	0.47	0.1	0.001	0.002	0.004	0.006	0.0209	0.0008	520	
PD21257	0.016	1.48	0.28	0.02	2.4	0.5	0.001	<0.001	0.001	0.006	0.005	0.0215	0.0012	560	
PD21258	0.024	1.42	0.24	0.14	2.84	0.44	0.225	0.004	0.003	0.01	0.01	0.0184	0.0024	510	140
PD21259	0.028	1.36	0.26	0.1	2.36	0.5	0.13	0.003	0.002	0.01	0.004	0.0167	0.0095	550	153
PD21260	0.028	1.32	0.26	0.13	2.24	0.47	0.181	0.003	0.002	0.006	0.005	0.018	0.0015	560	
PD21261	0.025	1.47	0.3	0.07	2.49	0.46	0.123	0.001	0.001	0.009	0.004	0.0196	0.0021	540	163
PD21262	0.02	1.48	0.24	0.05	3.41	0.47	0.106	0.002	0.002	0.006	0.008	0.0176	0.0006	480	
PD21263	0.025	1.35	0.27	0.09	2.53	0.49	0.127	0.001	0.002	0.008	0.006	0.0196	0.0021	530	176
PD21277	0.028	1.53	0.23	0.03	3.55	0.5	0.056	0.002	0.001	0.001	0.008	0.0174	0.0008	510	
PD21278	0.028	1.49	0.29	0.04	2.56	0.51	0.057	0.003	0.001	0.001	0.004	0.0182	0.0039	510	108

Appendix 2 – Welding details and mechanical properties.

LAB	PROC	POS	SHIELD GAS	PLATE TYPE	PLATE THICK (cm)	WIRE ID	WELD ID	dT/dt @538°C °C/s	YS Mpa	UTS Mpa	El %	%RA %	CVN 0°F j	CVN -60°F j
NSWC	GMAW-S	FLAT	C5	HSLA-100	5.08	Ltec2	JB-32	29	696	785			125	110
NSWC	GMAW-S	FLAT	C5	HSLA-100	5.08	CTC03N	JB-35	29	664	768	24	72	161	137
NSWC	GMAW-S	FLAT	C5	HSLA-100	5.08	CS2A	MV-10	29	779	882	11	62	60	34
NSWC	GMAW-S	FLAT	C5	HSLA-100	5.08	CS2A	MV-11	29	719	834	12	10	51	42
NSWC	GMAW-S	FLAT	C5	HSLA-100	5.08	CS2A	MV-12	29	668	779	12	67	37	12
NSWC	GMAW-S	FLAT	C5	HSLA-100	5.08	LTEC1	MV-13	29	703	861	11	69	130	118
NSWC	GMAW-S	FLAT	C5	HSLA-100	5.08	LTEC2	MV-14	29	723	868	12	67	146	139
EBDIV	GMAW-S	FLAT	C5	HY-80	1.91	ARC100N	PD21080	6	579	648	26	76	267	209
EBDIV	GMAW-S	FLAT	C5	HY-80	5.08	ARC100N	PD21081 S1	59	739	772	22	71	188	133
EBDIV	GMAW-S	FLAT	C5	HY-80	5.08	ARC100N	PD21081 S2	58	698	737	22	72	192	150
EBDIV	GMAW-P	VERT	C5	HSLA-100	5.08	ARC100N	PD21092 S1	42	726	758	22	76	245	211
EBDIV	GMAW-P	VERT	C5	HSLA-100	5.08	ARC100N	PD21092 S2	44	687	730	22	76	229	184
EBDIV	GMAW-S	FLAT	C5	HSLA-80	1.91	ARC100N	PD21149	11	620	668	25	77	256	221
EBDIV	GMAW-S	FLAT	C5	HSLA-80	0.95	ARC100N	PD21150	1	496	641	26	76	130	78
EBDIV	GMAW-S	FLAT	C5	HSLA-100	5.08	ARC100N	PD21151 S1	57	684	712	22	73	224	185
EBDIV	GMAW-S	FLAT	C5	HSLA-100	5.08	ARC100N	PD21151 S2	58	675	712	22	74	234	166
EBDIV	GMAW-P	VERT	C5	HSLA-80	0.95	ARC100N	PD21171	1	485	634	27	79	151	52
EBDIV	GMAW-P	VERT	C5	HSLA-80	1.91	ARC100N	PD21172	12	599	661	26	78	249	200
EBDIV	GMAW-P	VERT	C5	HSLA-80	1.91	ARC100N	PD21175	17	610	668	26	78	298	260
EBDIV	GMAW-S	FLAT	C5	HSLA-80	0.95	ARC100N	PD21176	6	574	648	27	81	203	167
EBDIV	GMAW-S	FLAT	C5	HY-80	1.91	ARC100N	PD21177	18	599	648	24	76	222	184
EBDIV	GMAW-P	VERT	C5	HY-80	1.91	ARC100N	PD21178	17	620	675	25	77	273	191
EBDIV	GMAW-S	FLAT	C5	HSLA-80	1.91	ARC100N	PD21202	18	613	648	25	76	302	193
EBDIV	GMAW-P	VERT	C5	HSLA-80	1.91	ARC100L	PD21215	12	579	651	25	77	240	196
EBDIV	GMAW-P	FLAT	C5	HSLA-80	1.91	ARC100L	PD21216	17	599	665	24	78	321	233
EBDIV	GMAW-S	FLAT	C5	HSLA-80	1.91	ARC100L	PD21217	12	568	634	23	77	222	107
EBDIV	GMAW-S	FLAT	C5	HSLA-80	0.95	CTC03N	PD21220	6	567	641	23	76	145	133
EBDIV	GMAW-S	FLAT	C5	HSLA-80	0.95	ARC100L	PD21222	1	501	622	23	76	115	33
EBDIV	GMAW-S	FLAT	C5	HY-80	1.91	CTC03N	PD21232	18	623	686	23	72	200	175
EBDIV	GMAW-P	VERT	C5	HY-80	1.91	CTC03N	PD21233	18	617	703	24	74	244	217
EBDIV	GMAW-S	FLAT	C5	HY-80	1.91	ARC100L	PD21234	18	627	679	24	75	219	175
EBDIV	GMAW-P	VERT	C5	HY-80	1.91	ARC100L	PD21235	18	586	661	24	75	236	169
EBDIV	GMAW-S	FLAT	C5	HSLA-80	2.54	ARC100N	PD21242	24	592	651	24	76	235	199
EBDIV	GMAW-S	FLAT	C5	HSLA-80	2.54	CTC03N	PD21243	24	579	655	24	77	206	149
EBDIV	GMAW-S	FLAT	C5	HSLA-100	5.08	ARC100R	PD21251 S1	58	866	907	17	64	173	149
EBDIV	GMAW-S	FLAT	C5	HSLA-100	5.08	ARC100R	PD21251 S2	58	870	919	18	68	182	149
EBDIV	GMAW-P	VERT	C5	HSLA-100	5.08	CTC03N	PD21252 S2	43	680	751	21	73	183	145
EBDIV	GMAW-S	FLAT	C5	HSLA-100	5.08	CTC03N	PD21253 S1	58	682	730	20	71	182	149

Appendix 2 (cont'd)

LAB	PROC	POS	SHIELD GAS	PLATE TYPE	PLATE THICK (cm)	WIRE ID	WELD ID	dT/dt @538°C °C/s	YS Mpa	UTS Mpa	El %	%RA %	CVN 0°F j	CVN -60°F j
EBDIV	GMAW-S	FLAT	C5	HSLA-100	5.08	CTC03N	PD21253 S2	58	689	744	20	67	165	130
EBDIV	GMAW-P	VERT	C5	HSLA-100	5.08	ARC100R	PD21254 S1	69	873	914	19	71	199	168
EBDIV	GMAW-P	VERT	C5	HSLA-100	5.08	ARC100R	PD21254 S2	71	847	903	19	70	211	162
EBDIV	GMAW-S	FLAT	C5	HSLA-80	1.91	ARC100N	PD21255	18	586	651	24	77	265	234
EBDIV	GMAW-S	FLAT	C5	HSLA-80	1.91	CTC03N	PD21256	18	592	658	23	74	191	162
EBDIV	GMAW-S	FLAT	C5	HSLA-80	1.91	ARC100L	PD21257	18	561	627	23	74	156	138
EBDIV	GMAW-P	VERT	C5	HSLA-80	0.97	CTC03N	PD21258	6	553	677	24	79	151	96
EBDIV	GMAW-P	VERT	C5	HSLA-80	0.97	ARC100L	PD21259	1	508	657	25	82	143	54
EBDIV	GMAW-P	VERT	C5	HSLA-80	0.97	ARC100L	PD21260	5	542	643	25	79	162	122
EBDIV	GMAW-P	VERT	C5	HSLA-80	1.91	ARC100N	PD21261	17	575	648	26	78	332	268
EBDIV	GMAW-P	VERT	C5	HSLA-80	1.91	CTC03N	PD21262	18	582	651	24	76	253	191
EBDIV	GMAW-P	VERT	C5	HSLA-80	1.91	ARC100L	PD21263	17	568	634	25	78	297	230
EBDIV	GMAW-P	VERT	C5	HSLA-80	2.54	CTC03N	PD21277	23	613	672	22	77	275	253
EBDIV	GMAW-P	VERT	C5	HSLA-80	2.54	ARC100N	PD21278	23	617	675	25	78	351	301

INITIAL DISTRIBUTION

Copies

2 ONR
- 1 Code 332 (Vasudevan)
- 1 Code 332 (Yoder)

6 NAVSEA
- 4 SEA 03M2
- 2 PMS450T4

1 NRL
- 1 Code 6234

2 DTIC

1 National Ctr for Excellence in Metalworking Technology

1 Navy Joining Center

2 General Dynamics, Elec Boat Div.
- 1 Code D341
- 1 Code D470

2 Newport News Shipbuilding
- 1 Code 037
- 1 Code E12

1 ESAB Welding and Cutting Products
- 1 Welding Consumables

1 Hobart Brothers Company
- 1 Filler Metal Engineering Dept

1 Lincoln Electric Company
- 1 Consumable Research and Development

1 Colorado School of Mines
- 1 Center for Welding and Joining

1 Oregon Graduate Institute
- 1 Dept of Matls Sci and Engin

DIVISION DISTRIBUTION

Copies	Code
1	0115 (Messick)
1	60
1	601
1	603
1	61
1	61s
1	611
1	612
1	613
1	614
1	614 (Czyryca)
1	62
1	63
1	64
1	65
1	66
1	67
1	68

BRANCH DISTRIBUTION

1	615
10	615 (Blackburn)
1	615 (DeLoach)
1	615 (Franke)
1	615 (Wong)